

Comb-like dextran copolymers: A versatile strategy to coat highly porous MOF nanoparticles with a PEG shell

Giovanna Cutrone, Jingwen Qiu, Mario Menendez-Miranda, Juan M Casas-Solvas, Ahmet Aykaç, Xue Li, Daniel Foulkes, Borja Moreira-Alvarez, Jorge R Encinar, Catherine Ladaviere, et al.

▶ **To cite this version:**

Giovanna Cutrone, Jingwen Qiu, Mario Menendez-Miranda, Juan M Casas-Solvas, Ahmet Aykaç, et al.. Comb-like dextran copolymers: A versatile strategy to coat highly porous MOF nanoparticles with a PEG shell. Carbohydrate Polymers, 2019, 223, pp.115085. 10.1016/j.carbpol.2019.115085 . hal-03009705

HAL Id: hal-03009705
https://hal.science/hal-03009705

Submitted on 3 Dec 2020

HAL is a multi-disciplinary open access archive for the deposit and dissemination of scientific research documents, whether they are published or not. The documents may come from teaching and research institutions in France or abroad, or from public or private research centers.

L'archive ouverte pluridisciplinaire **HAL**, est destinée au dépôt et à la diffusion de documents scientifiques de niveau recherche, publiés ou non, émanant des établissements d'enseignement et de recherche français ou étrangers, des laboratoires publics ou privés.

Comb-like dextran copolymers: A versatile strategy to coat highly porous MOF nanoparticles with a PEG shell

Giovanna Cutrone[a,1], Jingwen Qiu[b,1], Mario Menendez-Miranda[b], Juan M. Casas-Solvas[a], Ahmet Aykaç[a,2], Xue Li[b], Daniel Foulkes[b], Borja Moreira-Alvarez[c], Jorge R. Encinar[c], Catherine Ladavière[d], Didier Desmaële[e], Antonio Vargas-Berenguel[a,*], Ruxandra Gref[b,*]

[a] Department of Chemistry and Physics, University of Almería, Ctra. de Sacramento s/n, 04120 Almería, Spain

[b] Institut des Sciences Moléculaires d'Orsay, UMR CNRS 8214, Université Paris-Sud, Université Paris Saclay, 91400 Orsay, France

[c] Department of Physical and Analytical Chemistry, University of Oviedo, Julián Clavería 8, 33006 Oviedo, Spain

[d] University of Lyon, CNRS, UMR 5223, IMP, 15 bd André Latarjet, F-69622 Villeurbanne, France

[e] Institut Galien Paris-Sud, UMR 8612, CNRS, Université Paris-Sud, Faculté de Pharmacie, 5 rue JB Clément, 92296 Châtenay-Malabry, France

∗ Corresponding authors. E-mail addresses: avargas@ual.es (A. Vargas-Berenguel), ruxandra.gref@u-psud.fr (R. Gref).

1 These authors contributed equally.

2 Current address: Faculty of Engineering and Architecture Izmir Kâtip Çelebi University Çiğli 35620 Izmir Turkey.

Keywords: Metal organic frameworks nanoparticles, Surface modification, Dextran, Poly(ethylene glycol), Macrophage uptake, Click chemistry

Abstract. Nanoparticles made of metal-organic frameworks (nanoMOFs) are becoming of increasing interest as drug carriers. However, engineered coatings such as poly(ethylene glycol) (PEG) based ones are required to prevent nanoMOFs recognition and clearance by the

innate immune system, a prerequisite for biomedical applications. This still presents an important challenge due to the highly porous structure and degradability of nanoMOFs. We provide here a proof of concept that the surface of iron-based nanoMOFs can be functionalized in a rapid, organic solvent-free and non-covalent manner using a novel family of comb-like copolymers made of dextran (DEX) grafted with both PEG and alendronate (ALN) moieties, which are iron complexing groups to anchor to the nanoMOFs surface. We describe the synthesis of DEX-ALN-PEG copolymers by click chemistry, with control of both the amount of PEG and ALN moieties. Stable DEX-ALN-PEG coatings substantially decreased their internalization by macrophages in vitro, providing new perspectives for biomedical applications.

1. Introduction

Metal-organic frameworks (MOFs) are one of the latest classes of ordered porous solids which have attracted growing interest since their discovery in 1989 (Hoskins & Robson, 1989), in reason of their remarkable versatility. Indeed, almost any metal could be associated to polycomplexing linkers such as carboxylates, phosphonates, sulfonates or imidazolates leading to the discovery of thousands of MOFs with a variety of pore sizes and shapes (Horcajada et al., 2012; Liu et al., 2017; Yuan et al., 2018). Among the MOFs family, nanosized MOFs (nano- MOFs) based on porous iron(III) polycarboxylates have emerged as an important class of biodegradable and non-toxic (Horcajada et al., 2010; Baati et al., 2013) materials that can be loaded with exceptional quantities (within the 20–70 wt% range) of a large variety of therapeutic agents (Agostoni, Anand et al., 2013; Agostoni, Chalati et al., 2013; Horcajada et al., 2010). This paved the way to novel perspectives in terms of targeted delivery of drugs (Simon-Yarza et al., 2017; Simon- Yarza, Baati, Paci et al., 2016; Simon-Yarza, Baati, Neffati et al., 2016) and theranostics (Horcajada et al., 2010). For biomedical applications, it is of utmost importance to engineer the surface of the nanoMOFs, since the in vivo fate of any nanoparticles (NPs) in the living body (biodistribution, pharmacokinetics and targeting abilities) depends upon its surface physicochemical properties. For instance, it was shown that surface functionalization with hydrophilic polymers such as poly (ethylene glycol) (PEG) in a “brush” configuration could dramatically extend the blood circulation times of NPs by mitigating their recognition by the reticuloendothelial system (Gref et al., 1994, 1995). However, to date, Doxil® represents the only FDA-approved PEGylated liposome- based nanocarrier of anticancer drug (Doxorubicin) (Barenholz, 2012). Functionalization of nanoMOFs surfaces will be critical to their success as potential

nanocarriers in therapeutic contexts (Abdelhameed, Rehan, & Emam, 2018). However, thus far, only a limited number of cases have been reported that have aimed to modify the surface of nanoMOFs with PEG shells (Agostoni et al., 2015; Chen et al., 2017; Giménez-Marqués et al., 2018; Zhang et al., 2015; Zimpel et al., 2016). As compared to dense NPs made of biodegradable polymers or liposomes, the porous surface of MOFs is a challenging surface to functionalize. Indeed, it was reported that PEG chains are able to penetrate within the pores, blocking them and/or decreasing the drug loading capacity (Agostoni et al., 2015). To avoid PEG penetration into the highly porous MOFs, PEG-based shells were formed by GraftFast, a method involving polymerization of acryl PEGs (Giménez-Marqués et al., 2018). By this way, PEG derivatives with initial molecular weights of 480, 2000 and 5000 Da were polymerized leading to stable coatings. However, the molecular weight of the resulting PEG-based copolymer could not be efficiently controlled. Another recent strategy employed cyclodextrin (CD) derivatives, which were first adsorbed onto the MOFs surfaces prior to complex formation with PEG grafted with adamantane moieties (Agostoni et al., 2015). However, the two-step procedure required by this method resulted in a difficulty to control the quantity of grafted PEG.

Moreover, no study has yet demonstrated that a PEG coating on nanoMOFs could effectively reduce their reticuloendothelial sequestration. In this context, there is still a clear demand to engineer versatile PEG-based coatings onto the nanoMOFs surface, with proof of concept, by reducing uptake by macrophages. Here we address this challenge by using a novel family of copolymers, synthesized by grafting onto a dextran (DEX) backbone two types of moieties: i) PEG chains to avoid macrophage uptake and ii) alendronate (ALN) to spontaneously coordinate to the nanoMOFs surface. Iron trimesate MIL-100(Fe) (MIL stands for Material of the Institute Lavoisier) nanoMOFs were selected as core materials, in reason of their biodegradability, capacity to incorporate a series of drugs such as antibiotics (Li et al., 2019), anticancer drugs (Di Nunzio, Agostoni, Cohen, Gref, & Douhal, 2014; Rodriguez-Ruiz et al., 2015), and anti-infective agents (Agostoni, Anand et al., 2013; Agostoni, Chalati et al., 2013), reaching unprecedented payloads together with controlled releases, versatility in terms of drug loadings and lack of in vivo toxicity (Baati et al., 2013; Simon-Yarza, Baati, Paci et al., 2016; Simon-Yarza, Baati, Neffati et al., 2016).

Here we show the possibility to achieve stable coatings by a straightforward method, based on cooperative interactions between the ALN moieties and the external surface of MIL-100(Fe) nanoMOFs. Thus, we describe the synthetic strategies to control both PEG and ALN densities

on the DEX backbone, as well as the convenient one-step method to coat the nanoMOFs. The PEG "brush" efficiently reduced macrophage uptake as demonstrated by both microscopic investigations and quantitative determination of the amount of internalized nanoMOFs using inductively coupled plasma mass spectrometry (ICPMS).

2. Materials and methods

2.1. Chemicals and general methods

Thin layer chromatography (TLC) was performed on Merck silica gel 60 F254 aluminum sheets and developed by UV–vis light, iodine, 5% v/v sulfuric acid in ethanol, 5% w/v phosphomolybdic acid in ethanol, and 1% w/v potassium permanganate in aqueous 0.1% w/v NaOH containing 7% w/v potassium carbonate, depending on the case. Flash column chromatography was performed on Merck silica gel (230–400 mesh, ASTM). Infrared spectra were recorded on a Bruker Alpha FTIR equipped with a Bruker universal ATR sampling accessory. 1H, 13C, 31P and 2D NMR spectra were recorded on a Bruker Avance III HD 600 MHz spectrometer equipped with a QCI 1H/13C/15N/31P proton-optimized quadrupole inverse cryoprobe with ^{1}H and ^{13}C cryochannels, or a Bruker Nanobay Avance III HD 300 MHz spectrometer equipped with a QNP 1H/13C/19F/31P probe, depending on the sample. Standard Bruker software was used for acquisition and processing routines. Chemical shifts (δ) are given in parts per million (ppm) and referenced to internal tetramethylsilane (TMS) signal (δH, δC 0.00). J values are given in hertz (Hz). ESI-TOF mass spectra were recorded on an Agilent LC/MSD-TOF spectrometer in both positive and negative modes. Syringe filtering was conducted using nylon 0.45 μm Milipore Millex® syringe-driven filter units. Dialysis was performed using Medicell Membranes Ltd 12000–14000 Da molecular weight cutoff (MWCO) Visking dialysis tubing. Elemental analyses were recorded on an Elementar Vario Micro CHNS analyzer. HR-ICP-MS results were obtained by using a Termo Finningan magnetic sector field ELEMENT 2 inductively coupled plasma mass spectrometer. A Hanna HI 98,192 EC/TDS/NaCl/ Resistivity meter was employed to monitor dialysate solutions conductivity during dialysis.

6-Bromohexanoic acid (Aldrich, 97%), sodium azide (Panreac, 99%), N-hydroxysuccinimide (NHS, Aldrich, 98%), N-(3-dimethylaminopropyl)- N′-ethylcarbodiimide hydrochloride (EDC, Fluka, ≥98%), alendronic acid monosodium salt trihydrate (CarboSynth, purum), poly (ethylene glycol) methyl ether ($MeOPEG_{45}OH$, Aldrich, Mn ~2000), 4-dimethylaminopyridine (DMAP, Fluka, ≥98%), methanesulfonyl chloride (MsCl, Fluka,

≥99%), 1,1'-carbonyldiimidazole (CDI, Acros, 97%), propargylamine (Aldrich, 98%), anhydrous copper(II) sulfate (Fluka, 98%), (+)-sodium L-ascorbate (Sigma, BioXtra, ≥99%), and ethylenediaminetetraacetic acid disodium salt dihydrate (EDTA, Fluka, purum) were purchased from commercial sources and used without further purification otherwise indicated. Anhydrous LiCl (Sigma- Aldrich, 99%) and dextran T-40 (Pharmacosmos, purum, Nominative Mw 40,000 Da) were purchased from commercial sources and dried at 80 °C under high vacuum for 48 h in the presence of P2O5 prior to use. Triethylamine (Sigma-Aldrich,>99%) and organic solvents were dried according to literature procedures (Perrin & Armarego, 1989). Dry DMF (AcroSeal, 99.8%, over molecular sieves) was purchased from Acros. Iron (III) chloride hexahydrate (Alfa Aesar, Schiltigheim, France, 98%), 1,3,5-benzenetricarboxylic acid (BTC, Sigma-Aldrich, Saint-Quentin- Fallavier, France, 95%) and absolute ethanol (Carlo Erba, Val-de-Reuil, France, 99%) were used for the synthesis of nanoMOFs. Potassium chloride (Sigma-Aldrich) was used for nanoMOFs Zeta potential (ZP) measurements. Doxorubicin (DOX, Sigma-Aldrich, 98%) was used for drug encapsulation. Human serum albumin (HSA, Sigma-Aldrich) and bicinchoninic acid (BCA) protein assay kit (Pierce™ Thermo Fisher) was used for HSA adsorption test. Deionized Milli-Q water was obtained from a Millipore apparatus with a 0.22 μm filter.

The number average molecular weight (Mn) and the molar-mass dispersity values of dextran derivatives 5 and 7 were measured by using a SEC column (TSKgel G2500PW and G6000PW columns) coupled with a differential refractometer (RI, Optilab T-rEX, Wyatt Technology) with a laser at λ=658 nm, thermostated at 25 °C, and a multi-angle laser light scattering instrument (MALLS, HELEOS II, Wyatt Technology) equipped with a laser operating at λ=664 nm. Degassed and filtered (0.1 μm membrane) 0.15M ammonium acetate/0.20M acetic acid buffer (pH=4.5) was used as eluent at a flow rate of 0.5 mL/min (with a refractive index increment value, dn/dc of 0.147 ml/g for DEX). These eluents were also used as solvent of samples, and the resulting solutions were filtered on a 0.45 μm membrane before injection. Finally, 200 μL of each sample at 1 mg/mL were injected. The data have been exploited thanks to the ASTRA 6.1.7.17 software (Wyatt Technology). Murine macrophage cell line J774A.1 (ATCC) were grown in Dulbecco's Modified Eagle's Medium (Thermo Fischer) supplemented with 10% v/v decomplemented fetal bovine serum (FBS) at 37 °C in humidified conditions with 5% CO2. Prussian blue iron staining kit (Sigma-Aldrich) containing potassium ferrocyanide, pararosaniline and hydrochloric acid was used for cell staining.

2.2. Synthesis and characterization of dextran-PEG

2.2.1. Synthesis of 6-azidohexanoic acid (1)

Compound 1 was prepared as described in literature (Alemán, G. Cutrone, et al. *Carbohydrate Polymers 223 (2019) 115085* 2 Pedini, & Rueda, 2009; Kuil, Branderhorst, Pieters, De Mol, & Liskamp, 2009) with small modifications. Specifically, NaN3 (1 g, 15.4 mmol) was added to a solution of 6-bromohexanoic acid (1.5 g, 7.7 mmol) in dry DMF (10 mL) under N2 atmosphere and stirred at 85 °C overnight until TLC (2:1 hexane:EtOAc) showed complete disappearance of the starting material and the appearance of a spot at Rf=0.59. The solvent was rotary evaporated under high vacuum and the residue was dissolved in H2O (20 mL) and extracted with EtOAc (3 x 30 mL). The organic layers were combined, dried (MgSO4), and rotary evaporated to give 6-azidohexanoic acid 1 (0.866 g, 5.5 mmol, 70%) as slightly yellow oil. NMR data agreed with those previously reported (Kuil et al., 2009): 1H NMR (300 MHz, CDCl3) δ (ppm): 11.04 (s, 1H, COOH), 3.24 (t, 2H, ^{3}J = 6.9 Hz, CH_2N_3), 2.32 (t, 2H, ^{3}J = 7.3 Hz, CH_2CO_2H), 1.70-1.50 (m, 4H, $CH_2CH_2C\ O_2H$, $CH_2CH_2N_3$), 1.40 (m, 2H, $CH_2CH_2CH_2N_3$); ^{13}C NMR (75 MHz, $CDCl_3$) δ (ppm): 179.1 (CO_2H), 51.2 (CH_2N_3), 34.0 (CH_2CO_2H), 28.6 ($CH_2CH_2N_3$), 26.2 ($CH_2CH_2CH_2N_3$), 24.3 ($CH_2CH_2CO_2H$).

2.2.2. Synthesis of 2,5-dioxopyrrolidin-1-yl 6-azidohexanoate (2)

Compound 2 was prepared as described in literature (Grandjean, Boutonnier, Guerreiro, Fournier, & Mulard, 2005) with small modifications. Specifically, N-hydroxysuccinimide (520 mg, 4.5 mmol) was added to a solution of 6-azidohexanoic acid 1 (650 mg, 4.1 mmol) in dry CH2Cl2 (10 mL) under N2 atmosphere at room temperature and the mixture was stirred until complete solubilisation. Then, EDC (860 mg, 4.5 mmol) was added and the solution was stirred at room temperature until TLC (2:1 hexane:EtOAc) showed complete disappearance of the starting material and the appearance of a spot at Rf=0.41. After 16 h, the mixture was washed with 1 N HCl (2×15 mL) and saturated aq. NaHCO3 (2×15 mL). The aqueous layer was extracted with CH2Cl2 (2 x 10 mL). All organic phases were combined, dried (MgSO4), and rotary evaporated. The residue was purified by column chromatography using 2:1 hexane:EtOAc as eluent to yield compound 2 (790 mg, 3.1 mmol, 76%) as a colourless liquid. NMR data agreed with those previously reported (Grandjean et al., 2005): ^{1}H NMR (300 MHz, $CDCl_3$) δ (ppm): 3.23 (t, 2H, ^{3}J = 6.7 Hz, CH_2N_3), 2.75 (s, 4H, $COCH_2CH_2CO$), 2.56 (t, 2H, ^{3}J = 7.3 Hz, CH_2COO), 1.90-1.30 (m, 6H, $CH_2CH_2CH_2CH_2N_3$); ^{13}C NMR (75 MHz, $CDCl_3$) δ (ppm): 169.1

(N*C*OCH$_2$), 168.4 (COO), 51.1 (CH$_2$N$_3$), 30.8 (*C*H$_2$COO), 28.4 (CH$_2$), 25.9 (CH$_2$), 25.6 (2CO*C*H$_2$*C*H$_2$CO), 24.1 (CH$_2$).

2.2.3. Synthesis of the sodium salt of [4-(6-azidohexanamido)-1-hydroxy-1 -(hydroxy-oxido-phosphoryl)-butyl]phosphonic acid (3)

Aqueous 0.1M NaOH (~32 mL) was added dropwise to a suspension of alendronic acid monosodium salt trihydrate (0.83 g, 2.56 mmol) in MilliQ water (18 mL) until pH ~8.5, forming a clear solution. A solution of 2,5-dioxopyrrolidin-1-yl 6-azidohexanoate 2 (0.78 g, 3.1 mmol) in acetonitrile (18 mL) was added in four portions each 15 min. Before each portion, pH was measured and readjusted to ~8.5 with aqueous 0.1M NaOH if needed. The reaction mixture was stirred overnight at room temperature and then the solvent was rotary evaporated. The residue was purified by a short column chromatography using 5:1→2:1 CH3CN:H$_2$O as eluent to yield compound 3 (0.84 g, 2.05 mmol, 80%) as a white solid after lyophilising: FT-IR (KBr) ν/ cm−1: 3445, 2938, 2867, 2100, 1632, 1558, 1105, 913, 620, 551; ^{1}H NMR (600 MHz, D$_2$O) δ (ppm): 3.34 (t, 2H, ^3J = 6.9 Hz, CH$_2$N$_3$), 3.22 (t, 2H, ^3J = 6.8 Hz, CONHC*H*$_2$) 2.28 (t, 2H, ^3J = 7.5 Hz, C*H*$_2$CONH), 2.01-1.93 (m, 2H, CH$_2$C), 1.86-1.81 (m, 2H, C*H*$_2$CH$_2$C), 1.66-1.61 (m, 4H, C*H*$_2$CH$_2$CONH, C*H*$_2$CH$_2$N$_3$), 1.42-1.37 (m, 2H, C*H*$_2$CH$_2$CH$_2$N$_3$); ^{13}C NMR (150 MHz, D$_2$O) δ (ppm): 176.9 (CONH), 73.9 (t, $^1J_{CP}$ = 134.2 Hz, C(PO$_3$)$_2$), 51.0 (CH$_2$N$_3$), 40.0 (NHCH$_2$), 36.6 (*C*H$_2$CONH), 31.1 (*C*H$_2$C), 27.7 (*C*H$_2$CH$_2$N$_3$), 25.4 (*C*H$_2$CH$_2$CH$_2$N$_3$), 24.9 (*C*H$_2$CH$_2$CONH), 23.4 (t, $^3J_{CP}$ = 5.9 Hz, *C*H$_2$CH$_2$C); ^{31}P (242.9 MHz, D$_2$O) δ (ppm): 18.2 (C(PO$_3$)$_2$); [ESI-TOF-MS]$^-$ *m/z* calcd for C$_{10}$H$_{21}$N$_4$O$_8$P$_2$ 387.0840, found 387.0839; *m/z* calcd for C$_{10}$H$_{20}$N$_4$O$_8$P$_2$Na 409.0660, found 409.0657 [M − H]−; [ESI-TOF-MS]$^+$ *m/z* calcd for C$_{10}$H$_{22}$N$_4$O$_8$P$_2$Na 411.0816 found 411.0818 [M+H]+; *m/z* calcd for C$_{10}$H$_{21}$N$_4$O$_8$P$_2$Na$_2$ 433.0635, found 433.0643 [M+Na]+; *m/z* calcd for C$_{10}$H$_{20}$N$_4$O$_8$P$_2$Na$_3$ 455.0455 found 455.0465 [M − H + 2Na]+; m/ z calcd for C$_{10}$H$_{19}$N$_4$O$_8$P$_2$Na$_4$ 477.0274, found 477.0283 [M – 2H + 3Na]+.

2.2.4. Synthesis of 1-azido-1-deoxy-ω-O-methoxypentatetracontaethylene glycol (4)

A solution of MeOPEG$_{45}$OH (35 g, 17.375 mmol), DMAP (428 mg, 3.5 mmol) and distilled Et$_3$N (5.6 mL, 40.250 mmol) in CH$_2$Cl$_2$ (40 mL) was cooled to 0 °C under inert atmosphere. MsCl (2.7 mL, 35 mmol) was added dropwise over 15 min and the mixture was stirred at 0 °C during 30 min and then kept overnight at room temperature. The reaction mixture was then diluted with CH$_2$Cl$_2$ (50 mL), and washed with 5% v/ v aqueous HCl solution (3×50 mL) and brine (50 mL). The organic phase was dried over MgSO$_4$, filtered and concentrated under

reduced pressure to dryness. The solid was subsequently dissolved in dry DMF (40 mL) and NaN3 (2.276 g, 35 mmol) was added. The mixture was stirred at 60 °C for 24 h before the solvent was rotary evaporated under high vacuum. The residue was suspended in THF (20 mL), sonicated (5 min), and filtered off. The clear organic filtrate was rotary evaporated, and the resulting solid was suspended in Et_2O (50 mL), sonicated (5 min) and filtered. The solid was dissolved in H_2O (100 mL) and extracted with CH_2Cl_2 (3×100 mL). The organic phases were combined, dried ($MgSO_4$) and rotary evaporated, and the residue dried under vacuum to give compound 4 (26.225 g, 12.858 mmol, 74%) as a slightly yellow powder: FT-IR (KBr) ν/cm^{-1}: 2868, 2105, 1093, 948, 842, 729; ^{1}H NMR (300 MHz, D_2O) δ: 3.96-3.93 (m, $^1J_{H,C}$ = 143.4 Hz, ^{13}C satellite peak), 3.75-3.68 (m, 176H, OC*H*$_2$C*H*$_2$O), 3.65-3.61 (m, 2H, C*H*$_2$CH$_2$N$_3$), 3.53-3.49 (m, 2H, CH$_2$N$_3$), 3.49-3.46 (m, $^1J_{H,C}$ = 71.7 Hz, ^{13}C satellite peak), 3.38 (s, CH$_3$O); ^{13}C NMR (75 MHz, D_2O) δ: 71.7 (MeO*C*H$_2$), 70.3 (O*C*H$_2$*C*H$_2$O), 70.2 (MeOCH$_2$*C*H$_2$O), 70.0 (O*C*H$_2$CH$_2$N$_3$), 58.8 (OMe), 50.9 (CH$_2$N$_3$).

2.2.5. Synthesis of dextran propargylcarbamate (DEX-PC, 5)

LiCl (1 g) and dextran T-40 (4 g) were pre-dried at 80 °C in a high vacuum oven for 2 days in the presence of P2O5. The mixture was further dried by suspension in dry toluene (50 mL) and subsequent vacuum distillation at 50 °C. This azeotropic drying process with toluene was repeated twice, and then with anhydrous DMF (1×50 mL) followed by evaporation of the solvent through a rotary evaporator at 60 °C under high vacuum. The dry mixture was finally dissolved in anhydrous DMF (80 mL) and stirred at 80 °C for 1.5 h. The solution was cooled down to room temperature before carbonyldiimidazole (0.972 g, 6 mmol) was added, and stirred for 2.5 h. Propargylamine (3.85 mL, 60 mmol) was then added and the mixture stirred at room temperature for 24 h. The solvent volume was reduced to 60 mL by rotary evaporation and the solution was poured into isopropanol (0.9 L). The resulting pale yellow solid was collected by filtration and dissolved in H2O (100 mL), syringe filtered (0.45 μm) and dialyzed (12000–14000 Da MWCO) against distilled water, changing dialysate solution each 3 h until its conductivity was stable and below 1 μS/cm (3 days for final value of 0.90 μS/cm) to yield DEX-PC 5 (3.6 g) as a white solid after lyophilization: FT-IR (KBr) ν/cm^{-1}: 3420, 2930, 1709, 1639, 1530, 1461, 1419, 1346, 1264, 1156, 1041, 1014, 766, 549, 527; 1H NMR (600 MHz, D_2O) δ (ppm): 5.36 (d, $^3J_{1,2}$= 3.8 Hz, α(1→3,4) H-1), 5.21 (app bd, J_{app}= 2.8 Hz, α reducing end H-1, CH-OCONH), 5.06 (d, $^3J_{1,2}$ = 2.6 Hz, H-1^S), 5.01 (d, $^3J_{1,2}$ =3.0 Hz, α(1→6) H-1), 4.98 (bs, H- 1^S), 4.63 (d, $^3J_{1,2}$ =7.2 Hz, β reducing end H-1), 4.02-3.93 (m, H-3,6^a, CH$_2$C≡), 3.78-3.73 (m, H-5,6^b), 3.60 (dd, $^3J_{1,2}$ =3.0 Hz, $^3J_{2,3}$=9.7 Hz, H-2), 3.55 (t, ^3J

=9.4 Hz, H-4), 3.51 (t, ^{3}J =9.9 Hz, H- 4^{S}), 3.44 (t, ^{3}J =9.5 Hz, H-4^{S}), 3.03 (bs, ≡CH), 2.95 (bs, ≡CH), 2.69 (app bd, J_{app}=8.7 Hz, ≡CH); ^{13}C NMR (150 MHz, D_2O) δ (ppm): 157.9 (CO), 157.0 (CO), 99.3, 98.2, 97.7 (α(1→6) C-1), 95.6 (C-1S), 80.4-78.8 (C≡), 76.7, 73.4 (C-3), 73.2-73.1 (≡CH), 72.0, 71.4 (C-2), 71.0, 70.2 (C-5), 69.9, 69.5 (C-4), 67.7, 65.5 (C-6), 65.2, 60.5, 30.1 (CH_2C≡); Anal.: found C 40.90%, H 6.536%, N 1.42%. The number average molecular weight and the molar-mass dispersity were measured to be *Mn* = 35,240 g/mol and Đ=1.14, respectively (Figure S14A).

2.2.6. Synthesis of DEX-ALN75-PEG25 (6)

Pre-dried LiCl (90 mg, 2.123 mmol) and DEX-PC 5 (350 mg, 0.0079 mmol containing 0.397 mmol of propargyl groups) were dissolved in H2O (5 mL) and heated at 60 °C. A solution of sodium alendronate derivative 3 (127 mg, 0.298 mmol) in H2O (2 mL) was added, followed by a suspension of $CuSO_4$ (29 mg, 0.179 mmol) and sodium ascorbate (118 mg, 0.596 mmol) in H_2O (1 mL), and the mixture was stirred at 90 °C overnight. After cooling down to room temperature, azide 4 (809 mg, 0.397 mmol) and a suspension of CuSO4 (38 mg, 0.238 mmol) and sodium ascorbate (157 mg, 0.794 mmol) in H2O (0.8 mL) were subsequently added. The mixture was stirred for 22 h at 90 °C, then diluted with H2O (10 mL), filtered through filtering paper and then through a 0.45 μm syringe filter. Aqueous 0.1M NaOH was added until pH ∼7.0, followed by a solution of 10mM EDTA at pH 7.0 (20 mL). The pH was then monitored and kept at ∼7.0 with 0.1M NaOH for 24 h. The mixture was again filtered through 0.45 μm syringe filter, lyophilized, re-dissolved in the minimum amount of water and dialyzed (12000–14000 Da MWCO) against distilled water, changing dialysate solution each 3 h until its conductivity was stable and below 1 μS/cm (3 days for final value of 0.60 μS/cm) to yield DEX-ALN75-PEG25 6 (881 mg) as a brownish solid after lyophilization: FT-IR (KBr) ν/ cm−1: 3423, 2913, 2880, 1645, 1457, 1352, 1298, 1252, 1104, 1041, 952, 845, 548; ^{1}H NMR (600 MHz, D2O) δ (ppm): 8.03 (bs, H-5-C_2HN_3), 5.35 (bs, α(1→3,4) H-1), 5.27 (bs, α reducing H-1), 5.18 (app t, J_{app} = 5.0 Hz, C*H*-OCONH), 5.04 (bs, H-1^{S}), 5.00 (bs, α(1→6) H-1), 4.64 (bs, β reducing H-1), 4.51-4.44 (m, OCH_2CH_2-C_2HN_3), 4.40-4.38 (m, CH_2-C_2HN_3), 4.31-4.28 (m, $NHCH_2$-C_2HN_3), 4.02-3.93 (m, H-5,6^{a}), 3.87-3.84 (m, $^{1}J_{H,C}$ = 140.2 Hz, ^{13}C satellite peak), 3.73 (bs, H-3,6^{b}, OCH_2CH_2O), 3.67-3.64 (m, OCH_2CH_2-C_2HN_3), 3.61-3.60 (m, H-2), 3.56-3.52 (m, H-4), 3.45 (app t, J_{app} = 9.3 Hz, H-4^{S}), 3.40 (s, CH_3O), 3.34-3.19 (CH_2NH), 2.88 (bs, ≡CH), 2.78 (bs, ≡CH), 2.64 (bs, ≡CH), 2.23 (bs, CH_2CO), 1.93 (bs, CH_2C), 1.77 (bs, CH_2CH_2C), 1.61 (CH_2CH_2CO, CH_2CH_2-C_2HN_3), 1.30-1.16 (bs, $CH_2CH_2CH_2CO$); ^{31}P NMR (242.9 MHz, D_2O) δ (ppm): -1.4-(-2.6) ($C(PO_3)_2$); EA: found C

46.24%, H 7.582%, N 2.46%. HR-ICP-MS: found P 0.81%, Na 0.103%, Cu 1.05%, Li 0.042%.

2.2.7. Synthesis of DEX-ALN50-PEG50 (7)

Pre-dried LiCl (90 mg, 2.123 mmol) and DEX-PC 5 (350 mg, 0.0079 mmol containing 0.397 mmol of propargyl groups) were dissolved in H_2O (5 mL) and heated at 60 °C. A solution of sodium alendronate derivative 3 (85 mg, 0.198 mmol) in H_2O (1.5 mL) was added, followed by a suspension of $CuSO_4$ (19 mg, 0.119 mmol) and sodium ascorbate (79 mg, 0.397 mmol) in H_2O (1 mL), and the mixture was stirred at 90 °C overnight. After cooling down to room temperature, azide 4 (809 mg, 0.397 mmol) and a suspension of $CuSO_4$ (38 mg, 0.238 mmol) and sodium ascorbate (157 mg, 0.794 mmol) in H_2O (0.8 mL) were subsequently added. The mixture was stirred for 22 h at 90 °C, then diluted with H_2O (10 mL), filtered through filtering paper and then through a 0.45 μm syringe filter. Aqueous 0.1M NaOH was added until pH ∼7.0, followed by a solution of 10mM EDTA at pH 7.0 (20 mL). The pH was then monitored and kept at ∼7.0 with 0.1M NaOH for 24 h. The mixture was again filtered through 0.45 μm syringe filter, lyophilized, re-dissolved in the minimum amount of water and dialyzed (12000–14000 Da MWCO) against distilled water, changing dialysate solution each 3 h until its conductivity was stable and below 1 μS/cm (3 days for final value of 0.74 μS/cm) to yield DEX-ALN50-PEG50 7 (928 mg) as a brownish solid after lyophilization: FT-IR (KBr) ν/cm^{-1}: 3429, 2917, 2881, 1645, 1457, 1352, 1253, 1103, 952, 558; ^{1}H NMR (600 MHz, D_2O) δ (ppm): 8.03 (bs, H-5-C_2HN_3), 5.35 (bs, α(1→3,4) H-1), 5.26 (bs, α reducing H-1), 5.18 (app t, J_{app} = 5.0 Hz, C*H*-OCONH), 5.04 (bs, H-1^S), 5.00 (bs, α(1→6) H-1), 4.64 (bs, β reducing H-1), 4.47-4.43 (m, OCH_2CH_2-C_2HN_3), 4.40-4.38 (m, CH_2-C_2HN_3), 4.31-4.29 (m, $NHCH_2$-C_2HN_3), 4.02-3.93 (m, H-5,6^a), 3.87-3.84 (m, $^1J_{H,C}$ = 140.4 Hz, ^{13}C satellite peak), 3.73 (bs, H-3,6^b, OCH_2CH_2O), 3.67-3.64 (m, OCH_2CH_2-C_2HN_3), 3.61-3.59 (m, H-2), 3.56-3.52 (m, H-4), 3.43 (app t, J_{app} = 10.0 Hz, H-4^S), 3.41 (s, CH_3O), 3.32-3.18 (CH_2NH), 2.88 (bs, ≡CH), 2.70 (bs, ≡CH), 2.25 (bs, CH_2CO), 1.93 (bs, CH_2C), 1.78 (bs, CH_2CH_2C), 1.61 (CH_2CH_2CO, CH_2CH_2-C_2HN_3), 1.26 (bs, $CH_2CH_2CH_2CO$); ^{31}P NMR (242.9 MHz, D_2O) δ (ppm): -1.8-(-2.9) ($C(PO_3)_2$); EA: found C 46.85%, H 7.769%, N 2.27%. HR-ICP-MS: found P 0.57%, Na 0.060%, Cu 0.74%, Li 0.027%. The number average molecular weight and the molar-mass dispersity were measured to be *Mn* = 83,120 g/mol and Đ=1.36, respectively (Figure S14B).

2.2.8. Synthesis of DEX-ALN25-PEG75 (8)

Pre-dried LiCl (90 mg, 2.123 mmol) and DEX-PC 5 (350 mg, 0.0079 mmol containing 0.397 mmol of propargyl groups) were dissolved in H_2O (5 mL) and heated at 60 °C. A solution of sodium alendronate derivative 3 (43 mg, 0.100 mmol) in H_2O (1 mL) was added, followed by a suspension of $CuSO_4$ (10 mg, 0.060 mmol) and sodium ascorbate (40 mg, 0.200 mmol) in H_2O (1 mL), and the mixture was stirred at 90 °C overnight. After cooling down to room temperature, azide 4 (809 mg, 0.397 mmol) and a suspension of $CuSO_4$ (38 mg, 0.238 mmol) and sodium ascorbate (157 mg, 0.794 mmol) in H_2O (0.8 mL) were subsequently added. The mixture was stirred for 22 h at 90 °C, then diluted with H_2O (10 mL), filtered through filtering paper and then through a 0.45 μm syringe filter. Aqueous 0.1M NaOH was added until pH ∼7.0, followed by a solution of 10mM EDTA at pH 7.0 (20 mL). The pH was then monitored and kept at ∼7.0 with 0.1M NaOH for 24 h. The mixture was again filtered through 0.45 μm syringe filter, lyophilized, re-dissolved in the minimum amount of water and dialyzed (12000–14000 Da MWCO) against distilled water, changing dialysate solution each 3 h until its conductivity was stable and below 1 μS/cm (2 days for final value of 0.63 μS/cm) to yield DEX-ALN25-PEG75 8 (978 mg) as a brownish solid after lyophilization: FT-IR (KBr) ν/cm^{-1}: 3423, 2912, 2880, 1645, 1457, 1352, 1299, 1253, 1104, 1042, 1019, 951, 845, 550; ^{1}H NMR (600 MHz, D_2O) δ (ppm): 8.03 (bs, H-5-C_2HN_3), 5.35 (bs, α(1→3,4) H-1), 5.27 (bs, α reducing H-1), 5.19 (app t, J_{app} = 5.0 Hz, C*H*-OCONH), 5.05 (bs, H-1^S), 5.00 (bs, α(1→6) H-1), 4.90 (bs, H-1^S), 4.64 (bs, β reducing H-1), 4.64 (bs, OCH_2CH_2-C_2HN_3), 4.40-4.38 (m, CH_2-C_2HN_3), 4.31-4.28 (m, $NHCH_2$-C_2HN_3), 4.02-3.93 (m, H-5,6^a), 3.85-3.84 (m, $^1J_{H,C}$ = 140.4 Hz, ^{13}C satellite peak), 3.73 (bs, H-3,6^b, OCH_2CH_2O), 3.68-3.64 (m, OCH_2CH_2-C_2HN_3), 3.61-3.59 (m, H-2), 3.56-3.52 (m, H-4), 3.45 (app t, J_{app} = 9.6 Hz, H-4^S), 3.41 (s, CH_3O), 3.32-3.19 (CH_2NH), 3.02 (bs, ≡CH), 2.95 (bs, ≡CH), 2.23 (bs, CH_2CO), 1.93 (bs, CH_2C), 1.78 (bs, CH_2CH_2C), 1.61 (CH_2CH_2CO, CH_2CH_2-C_2HN_3), 1.31-1.22 (bs, $CH_2CH_2CH_2CO$); ^{31}P NMR (242.9 MHz, D_2O) δ (ppm): 0.5-0.1, -1.5-(-2.4) ($C(PO_3)_2$); EA: found C 47.86%, H 7.842%, N 2.05%. HR-ICP-MS: found P 0.26%, Na 0.092%, Cu 0.42%, Li 0.048%.

2.3. Synthesis and characterization of MIL-100(Fe) nanoMOFs

Iron trimesate nanoMOFs were synthesized using a microwave-assisted hydrothermal method as previously described (Agostoni, Anand et al., 2013; Agostoni, Chalati et al., 2013). Briefly, 30 mL of an aqueous mixture containing 6.0mM iron chloride hexahydrate and 4.0mM of 1,3,5-benzenetricarboxylic acid was heated at 130 °C under stirring prior to microwave irradiation at 1600W (Mars-5, CEM, USA). The synthesized nanoMOFs were recovered by centrifugation at 10,000 g for 15 min and purified by washing six times with absolute ethanol. Their morphology was observed with a transmission electron microscope (TEM, JEOL 1400

(120 kV), Japan). Mean hydrodynamic diameters and size distributions were determined by dynamic light scattering (DLS, Malvern Nano-ZS, Zetasizer Nano series, France). NanoMOFs' Zeta potential (ZP) was measured at 25 °C using a Zetasizer Nano-ZS G. Cutrone, et al. *Carbohydrate Polymers 223 (2019) 115085* 4 instrument in a pH range of 1–10. For this, nanoMOFs were diluted to a final concentration of 100 μg/mL using a 1mM KCl solution. The nanoMOFs specific surface area was measured by nitrogen sorption experiments at −196 °C on an ASAP 2020 (Micromeritics, USA) after sample degassing at 100 °C for 15 h under high vacuum. X-ray powder diffraction patterns (XRPD) were recorded for crystallinity characterization. NanoMOFs were stored in ethanol at room temperature and resuspended in aqueous media whenever needed.

2.4. Surface modification of MIL-100(Fe) nanoMOFs and their characterization

2.4.1. Preparation and characterization of DEX-ALN-PEG coated nanoMOFs

NanoMOFs were centrifuged at 10,000 g for 10 min to remove the storage solvent (ethanol) and then re-dispersed in water by vortex. For coating, they were incubated overnight at room temperature with DEXALN- PEG solutions at mass ratios DEX-ALN-PEG: nanoMOFs of 1:4, 1:2 and 1:1. The non-attached DEX-ALN-PEG fraction was removed by centrifugation (10,000 g, 10 min). The pellets were dried and the adsorbed DEX-ALN-PEG was quantified by ICP-MS. Briefly, nanoMOFs before and after modification with DEX-ALN-PEG were digested using aqua regia (15 min under ultrasonic bath), and phosphorous (P) quantification was performed using an ICP-MS equipped with a triple quadrupole (Agilent 8800, Agilent Technologies, Japan). Operation conditions were daily optimized using a tuning solution. P isotope was detected using "mass shift mode" (^{47}PO+) after reaction with oxygen in the cell. Conversely, scandium (Sc) (added as internal standard on samples and calibration standards solutions at a concentration of 10 μg/ L)) was detected using "on mass mode" (^{45}Sc+). Oxygen was introduced into the collision/reaction cell at a flow rate of 0.35 mL/min. Dwell time for each of the targeted isotopes was 1 s. P was quantified using external calibration using certified 1000 mg/L P standard solution (Merck, Germany).

The amount (A) of DEX-ALN-PEG associated to nanoMOFs was calculated on the basis of their P content by Eq. (1):

$$A = P1/P2 \times 100\% \quad (1)$$

where P1 (wt%) is the phosphorous content in the coated nanoMOFs and P2 (wt%) is the phosphorous content in the synthesized DEX-ALNPEG copolymers.

DEX-ALN-PEG coated nanoMOFs were characterized the same as the uncoated samples to determine their size distribution, morphology, porosity (BET surface area) and surface charge. The crystallinity of DEX-ALN-PEG coated nanoMOFs was studied by XRPD.

2.4.2. Colloidal stability investigation

Colloidal stabilities of DEX-ALN-PEG coated nanoMOFs were estimated by DLS after incubation in both MilliQ water and cell culture medium (DMEM complemented with 10% FBS, 1% penicillin/streptomycin (100 mg/mL) and 1% L-glutamine). Mean hydrodynamic diameters were measured at 6 h, and 1, 2, 4, 7, 9, 14, 18 and 21 d storage at 4 °C in water, and at 0, 2, 4, 6, and 8 h after incubation at 37 °C in cell culture media.

2.4.3. Effect of surface modification on drug encapsulation

MIL-100(Fe) nanoMOFs ethanolic suspension was first centrifuged (10 min, 10,000 g) to recover the sedimented nanoMOFs, which were further redispersed in pure water. For the DOX encapsulation, nanoMOFs aqueous suspension was mixed with DOX and gently stirred for 48 h at room temperature. The weight ratio between DOX and nanoMOFs was 1:5. The DOX loaded nanoMOFs were recovered by centrifugation (10,000 g, 10 min) and the supernatant was used to quantify the drug payload, which was calculated by Eq. (2):

$$Payload\ (\%) = \frac{Encapsulated\ Drug(mg)}{nanoMOFs(mg)} \times 100 \qquad 2$$

The DOX loaded nanoMOFs were further surface modified with DEX-ALN25-PEG75 8 by incubating the drug loaded nanoMOFs with DEX-ALN25-PEG75 8 aqueous solution overnight at mass ratio DEX-ALNPEG: nanoMOFs 1:1. After surface functionalization, the DEX-ALN25- PEG75 8 coated drug loaded nanoMOFs were recovered again by centrifugation (10 min, 10,000 g). The supernatant was also recovered to quantify the DOX amount.

2.4.4. Human albumin adsorption studies

NanoMOFs coated or not with DEX-ALN-PEG (300 μg/mL) were incubated with HSA solutions at 100 μg/mL in 10mM phosphate buffer (PB) at 37 °C. The samples were centrifuged at 10,000 g for 5 min to recover the nanoMOF pellets after 1, 2, 3, 4, 6, 8 and 12 h

incubation. The excess of HSA in the supernatant was quantified using a bicinchoninic acid (BCA) assay.

2.4.5. "Stealth" effect of the DEX-ALN-PEG shell

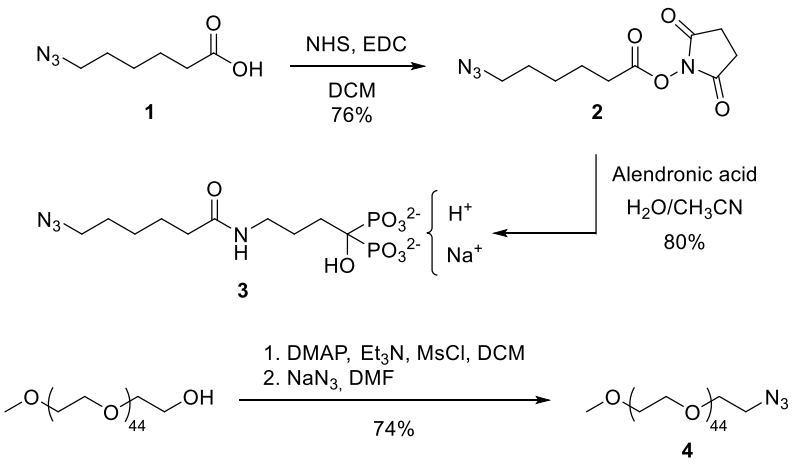
A direct visualization of the MIL-100(Fe) nanoMOFs inside J774A.1 macrophages was achieved based on iron staining using a Prussian blue staining kit. In a 24-well plate (with cover slips) 1×105 J774A.1 macrophages were placed with RPMI complete medium and 10% FBS. Each well of macrophages was treated with 50 μg of nanoMOFs, either coated or not with DEX-ALN-PEG. The macrophages were subsequently incubated for 2 and 4 h in an incubator at 37 °C with a CO2 concentration of 5%. Afterwards the wells were washed with complete medium and then further washed twice with PBS. Cells were fixed with 4% paraformaldehyde, washed and incubated for 10 min with 2% potassium ferrocyanide in 0.6mM hydrochloric acid. Cells were washed again with PBS, counterstained with pararosaniline hydrochloride (0.02%) and placed on a glass slide. A drop of emersion oil was applied to each coverslip and evaluated for iron staining using light microscopy. For Fe quantification by ICP-MS, macrophage cells (J774A.1) were seeded overnight at a density of 3.0×105 cells per well in 24-well plates in cell culture medium at 37 °C in 5% CO2. Cells were then incubated with 1 mL cell culture media containing nanoMOFs coated or not with DEX-ALN-PEG for 2, 4 and 6 h (nanoMOFs concentration=50 μg/mL). After incubation, the cells were washed with PBS for three times to eliminate the nanoMOFs which did not interact with the cells. Cells were finally dried and digested using aqua regia (15 min under ultrasonic bath). Fe quantification was performed using an ICP-MS equipped with a triple quadrupole (Agilent 8800). Operation conditions were daily optimized using a tuning solution. Fe and Co isotopes (added as internal standard on samples and calibration standards at a concentration of 10 μg/L) were detected using "on-mass mode" (54Fe+, 56Fe+, 59Co+). Helium was introduced into the collision/ reaction cell at a flow rate of 3 mL min–1. Dwell time for each of the targeted isotopes was 1 s. Fe was quantified using external calibration prepared using certified 1000 mg/L Fe standard solution (Merck, Germany).

3. Results and discussion

3.1. Synthesis and characterization of DEX-ALN-PEG copolymers

For the post-synthetic modification of the surface of MIL-100(Fe) nanoMOFs we planned to prepare DEX derivatives appended with alendronate (ALN) moieties and PEG chains. For this

strategy, we first prepared alendronate and PEG azide derivatives 3 and 4, respectively (Scheme 1). We then appended them on dextran T-40 grafted with a controlled number of therminal alkyne residues in the form of propargyl carbamate groups (DEX-PC 5) (Scheme 2) through a Cu(I)-catalyzed azide-alkyne cycloaddition (CuAAC) reaction to yield DEX-ALNPEG conjugates **6–8**.



Scheme 1. Synthesis of azide derivatives **3** and **4**.

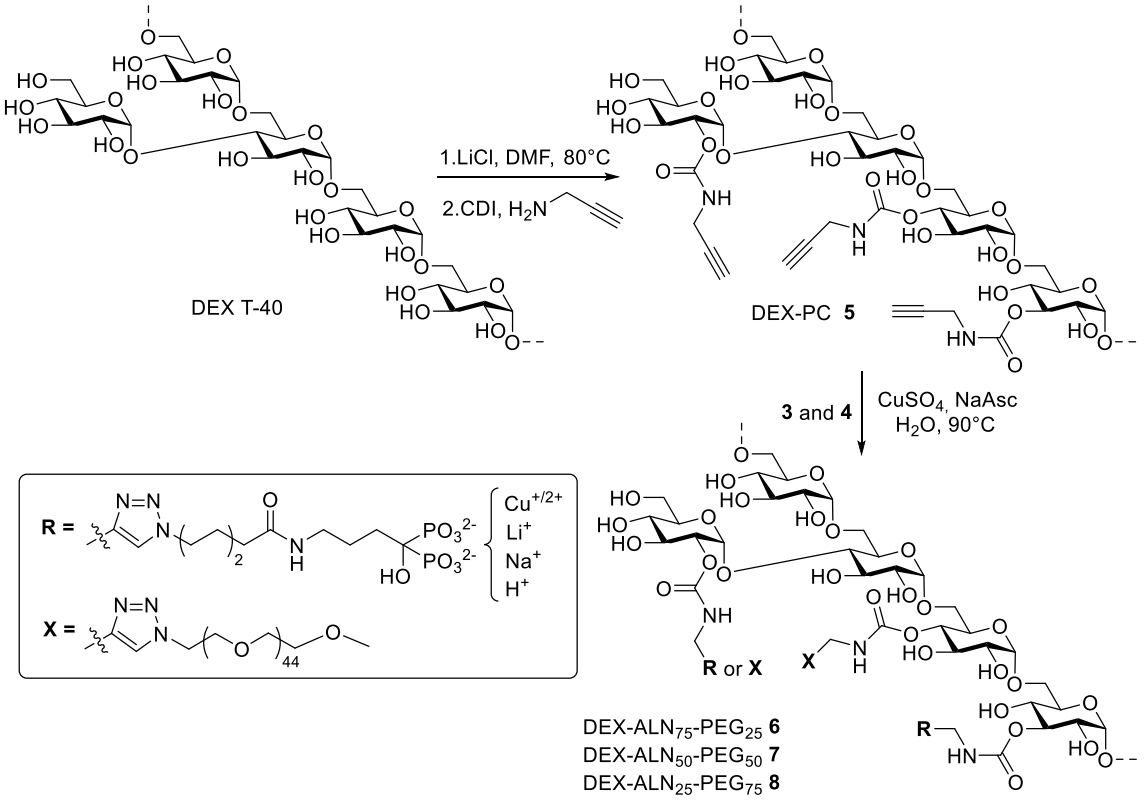
First, we synthesized azide alendronate derivative 3 (Scheme 1). The reaction between NHS-ester **2** and alendronic acid monosodium salt was performed in a MeCN:H_2O mixture keeping the pH at ~8.5 in order both to ensure the solubility of the alendronate salt and to guarantee the nucleophilic properties of the primary amine. However, precipitation of the crude after solvent evaporation with EtOH afforded product **3** with N-hydroxysuccinimide (NHS) byproduct, as confirmed by 1H NMR spectra. Attempts to remove NHS by solid-liquid extraction using organic solvents, including EtOAc and CH_3CN, failed. Thus, compound **3** was finally isolated by column chromatography using 5:1 CH_3CN:H_2O as initial eluent until NHS was washed out of the column, and 2:1 CH_3CN:H_2O for eluting pure 3 in 80% yield after lyophilization. In the initial alkaline pH ~8.5 environment, product 3 should be most likely in a trisodium salt form (Ke et al., 2016). However, flash column chromatography probably changed the distribution curves of the species in equilibrium by partial acidification of the mixture. Indeed, negative ESI-TOF mass spectrum depicted the species [M – Na]− and [M − H]− considering M as the monosodium salt. Similarly, positive ESITOF mass spectrum showed [M+H]+, [M+Na]+, [M − H + 2Na]+ and [M – 2H + 3Na]+, suggesting that the alendronate derivative was obtained mainly as the monosodium salt species.

Synthesis of azido PEG chain **4** was performed in two sequential steps. Commercial MeOPEG45OH, having a methoxy group at one end of the chain, was mesylated and used without any further purification for the reaction with sodium azide in DMF. Azido PEG 4 was isolated by two subsequent filtration processes with THF and Et2O that yielded 4 pure enough, as confirmed by NMR analysis. It is important to remark that the broad signal observed at δ 3.65-3.61 ppm corresponding to the main chain methylene groups appeared along with 13C satellites due to the 13C-1H coupling typically observed in high molecular weight PEG derivatives (Semple, Sullivan, Vojkovsky, & Sill, 2016).

The partial alkynylation of the dextran T-40 was achieved upon treatment with carbonyldiimidazole (CDI) and propargylamine forming propargyl carbamate groups on some of the free OH groups of the polysaccharide (Sun et al., 2011). DEX T-40 was extensively dried to minimize unwanted side reactions with water. Reaction was performed in dry DMF in the presence of anhydrous LiCl to help solubilizing the polysaccharide by interfering with its high crystallinity. DEX T-40 was then subsequently treated with 60 equivalents of CDI and an excess of propargylamine to give DEX-PC 5 (Scheme 2). Taking into account that the number of propargyl carbamate appendages directly depends on the CDI ratio, we expected these amounts to yield a maximum of 60 alkynes per DEX T-40 molecule. After dialysis and lyophilization, the composition of the obtained material was determined by elemental analysis. A mathematical model (see supplementary material) was developed to estimate the number of propargyl groups grafted on the polymer from those data. The model consistently estimated ∼50 propargyl carbamate groups each time the reaction was repeated. The functionalization of the polysaccharide can be observed by ^{1}H NMR through the appearance of broad signals at δ 3.03, 2.95 and 2.69 ppm that correspond to the ethynyl proton of propargyl carbamate groups located at different positions on the glucose moieties. In addition, a set of new signals arose from the substituted glucose units, namely a doublet at δ 5.06 ppm and broad singlet δ 4.98 ppm corresponding to anomeric protons, along with two triplets at δ 3.51 and 3.44 ppm assigned to the H-4 protons. In ^{13}C NMR spectrum, signals at δ 157.9-157.0 ppm indicated the presence of carbonyl groups on the structure, while the quaternary and ternary carbons of the ethynyl group gave peaks in the range of δ 80.4-78.8 and δ 73.2-73.1 ppm, respectively.

Once DEX-PC 5 was prepared, azides **3** and **4** were conjugated using CuSO**4** and sodium ascorbate as catalyst system at 90 °C in water (Scheme 2). Three dextran derivatives with different ratios of ALN and PEG branches were prepared, namely DEX-ALN75-PEG25 6,

DEX-ALN50- PEG50 7 and DEX-ALN25-PEG75 8, in order to study the effect of such ratio on both the stability of the coating and the "stealth" abilities of the resulting surface-modified nanoMOFs. To prevent that the different diffusion coefficients and reactivity kinetics of structurally so different azides as **3** and **4** might condition the actual ratio on 6–8, conjugations were performed sequentially starting with the required amount of alendronate derivative 3, followed after 8 h by addition of an excess of PEG azide 4. It was expected that the conjugation of the short chain of alendronate in the first place would not hinder the subsequent approach of the much bulkier PEG chain in the second step, which might occur if performed in the opposite order. Purification of 6–8 was carried out by washing with a solution of EDTA at pH ~7.0 in order to chelate the excess of copper, followed by dialysis against water using 12–14 KDa MWCO membranes until stable conductivity (< 1 μS/cm) was obtained in the dialysate solution.



Scheme 2. Synthesis of DEX-PC 5 and DEX-ALN-PEG 6–8. Structures of copolymers 5–8 are intended to simply depict different modes of carbamate attachment to the DEX chain and do not reflect either the actual spatial distribution of the appendages or the degree of substitution along the chain.

The analysis of number average molecular weights (Mn) of polymers before (DEX-PC 5) and after (DEX-ALN50- PEG50 7) chemical modification by PEG chains was achieved by SECMALLS. The starting material, DEX had a Mn value of 31,150 g/mol (Figure S14C). It was further shown that grafting ALN and PEG resulted in an expected increase of number average molecular weight (from 35,240 for DEX-PC **5** to 83,120 g/mol for DEX-ALN50-PEG50 **7**). This difference of around 50,000 g/mol could correspond to a ratio of 25% of PEG grafted chains of 2000 g/mol (since 50% × 2000 g/mol × 100 units=100,000 g/mol). Nevertheless, note that this determination presents a high uncertainly notably due to the hypothesis that the refractive index increment value of DEX-ALN50-PEG50 7 was equal to the one of unmodified dextran (dn/dc = 0.147 ml/g). Consequently, elemental analysis and HR-ICP-MS of the obtained copolymers was carried out in order to obtain a more accurate compositional profile for DEXALN- PEG derivatives 6–8. The mathematical model constructed to analyze these data (see supplementary material) indicated that only 66–74% of propargyl carbamates underwent cycloaddition (Table 1). Interestingly, the average number of ALN branches appended to the polysaccharide consistently changed depending on the initial ratio of reagents although in lesser extension than foreseen, varying from ∼15 in the case of DEX-ALN75-PEG25 6 to ∼5 for DEX-ALN25-PEG75 8. In sharp contrast, the average number of PEG branches only varies from ∼26 in the case of PEG-ALN75-PEG25 6 and ∼32 for DEX-ALN25-PEG75 8. This fact suggests that cycloaddition of PEG azide derivative 4 onto DEX-PC 5 is mainly limited by steric hindrance of the resulting product more than the reagent amount added to the reaction. The robustness of the model is evidenced by the fact that the sum of free propargyl carbamate (n), ALN (x) and PEG (z) branches keeps around 50 (±12%), which matches the estimated number of propargyl carbamate groups originally present in DEX-PC 5 starting material. It should be underlined that the model predicts the presence of at least one Cu atom per alendronate branch, along with an extra cation of Na and/or Li, even after extraction with EDTA prior dialysis. This result is not surprising since it is known that alendronate can chelate Cu(II) in a wide range of pH (Oms et al., 2016; Ostović, Stelmach, & Hulshizer, 1993), and indeed may explain the reduced cycloaddition efficiency for alendronate branches since copper cations could have been sequestered during the reaction. Although free, unbound Cu(II) has been demonstrated to be toxic for living cells (Biaglow, Manevich, Uckun, & Held, 1997), it requires concentrations as high as 78.5 μmol/L (5 mg/L) in serum for systemic toxicity in humans (Barceloux, 1999). Furthermore, the toxicity of chelated copper is remarkably lower, allowing its use to perform CuAAC reactions within living systems (Notni & Wester, 2016; Su, Li, Wang, Wang, & Zhang, 2016). We

observed that copper present in DEXALN- PEG **6–8** did not hinder MIL-100(Fe) coating (see below) which took place through their alendronate branches, and most likely, it was displaced by iron(III) atoms from nanoMOFs surface and washed out during centrifugation isolation. The proposed structures for 6–8 were demonstrated by 1H NMR spectra, where the formation of 1,2,3-triazole residues caused the appearance of a broad signal at δ 8.03 ppm in the three cases. In addition, methylene protons of PEG residues gave an intense peak at δ 3.73 ppm, while weak and broad singlets observed between δ 2.25 and 1.26 ppm evidenced the presence of alendronate branches. Furthermore, signals from non-reacted ethynyl protons were still notorious between δ 3.02 and 2.64 ppm, as the compositional model had predicted (Table 1). ^{13}C NMR experiments were strongly dominated by the high signals arising from PEG methylenes, which hindered both their acquisition and assignation. Finally, ^{31}P NMR confirmed the presence of phosphorus nuclei in the molecules with signals at δ 0.5-(-2.6) ppm.

Table 1

Calculated (see supplementary material) num

Derivative	*n* *Nb of propargyl groups*	*x* *Nb of ALN groups*	*z* *Nb of PEG chains*	*n+x+z*
DEX-PC **5**	50.1	0	-0.1	50.1
DEX-ALN$_{75}$-PEG$_{25}$ **6**	16.1	14.3	26.0	56.4
DEX-ALN$_{50}$-PEG$_{50}$ **7**	13.7	10.8	30.5	55.0
DEX-ALN$_{25}$-PEG$_{75}$ **8**	17.6	4.9	32.3	54.8

[a]An error of ±12% was estimated.

3.2. MIL-100(Fe) nanoMOFs synthesis and surface modification

3.2.1. DEX-ALN-PEG coating and physicochemical characterization

MIL-100(Fe) nanoMOFs with a mean hydrodynamic diameter of 191 ± 23 nm and BET (Brunauer, Emmett and Teller) surface area of 1690 ± 80 m2 g−1 were successfully synthesized by an organic solvent- free microwave-assisted hydrothermal method. They exhibited a facetted morphology (Fig. 1C), crystalline structure (Fig. 1B) and composition in

agreement with previously reported data (Agostoni, Anand et al., 2013; Agostoni, Chalati et al., 2013; Agostoni et al., 2015). Surface modification of MIL-100(Fe) nanoMOFs with DEX-ALN-PEG was carried out through a simple, “green” (meaning organic solventfree) method consisting on simple impregnation of nanoMOFs in aqueous solutions of the synthesized copolymers (Fig. 1A). The three copolymers with increased PEG contents, namely DEX-ALN75-PEG25 6, DEX-ALN50-PEG50 7, and DEX-ALN25-PEG75 8 were used for the surface modification.

The amount of DEX-ALN-PEG associated to the nanoMOFs was determined by ICP-MS by direct quantification of the P content in the coated samples. Indeed, P is the only element present in the DEX-ALNPEG copolymers, but not in the nanoMOFs, offering a straightforward and precise quantification method. It was found that after overnight incubation, amounts of DEX-ALN75-PEG25 6, DEX-ALN50-PEG50 7, and DEX-ALN25-PEG75 8 associated to the nanoMOFs reached 29 ± 2 wt%, 27 ± 2 wt% and 32 ± 3 wt%, respectively. Interestingly, these amounts of coating material attached to the nanoMOFs were among the highest reported so far. This efficient association could be possibly attributed to: i) the strong affinity of ALN for iron site at the surface and ii) the cooperative effects of ALN moieties as schematized in Fig. 1A. As comparison, cyclodextrin (CD)-phosphate coating on the same MIL- 100(Fe) nanoMOFs reached ∼17 wt%. In that case, only 3–4 phosphate moieties were attached to each CD (Aykaç et al., 2017). Indeed, alendronate, used mainly for osteoporosis treatment, is known to have a strong affinity for metals. It was incorporated in nanoMOFs made of Zrbased UiO-66 NPs (Zhu et al., 2014). It was highlighted that this amino-bisphosphonate was probably strongly anchored to the Zr-O clusters of the UiO NPs, thus promoting both high loading efficiencies (close to 100%) and controlled release.

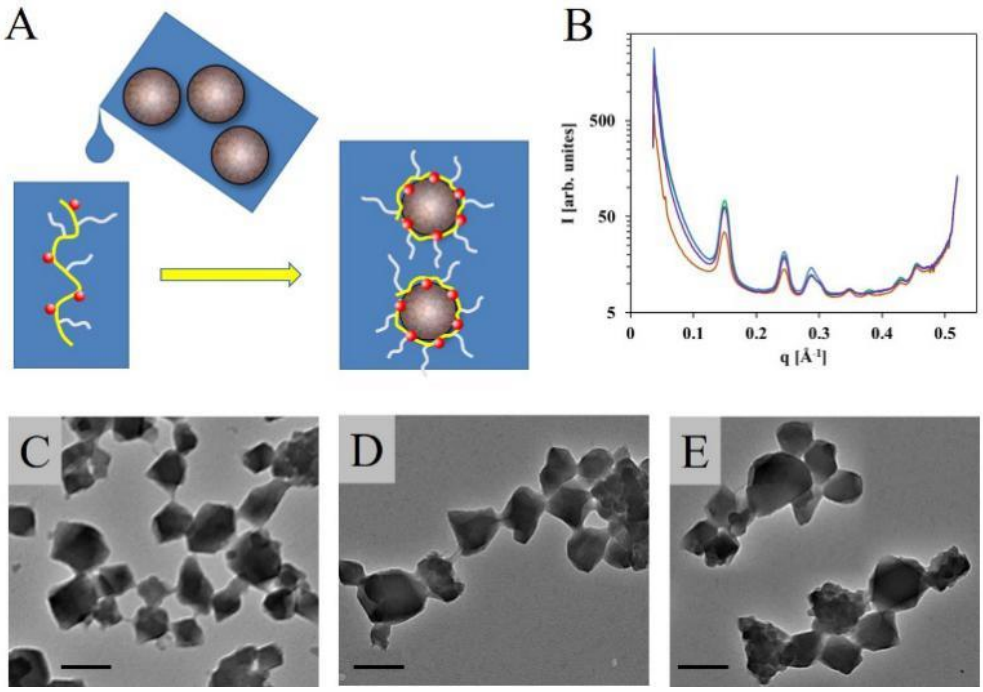


Fig. 1. Preparation and characterization of nanoMOFs coated or not with DEX-ALN-PEG. A: schematic representation of the «green» preparation of DEX-ALN-PEG coated nanoMOFs in water; For DEX-ALN-PEG, the red balls represent alendronate (ALN) moieties, dextran (DEX) is represented in yellow and poly(ethylene glycol) (PEG) chains are in white. B: XRPD patterns of nanoMOFs coated or not with DEX-ALN-PEG (green: nanoMOFs; purple: DEX-ALN75-PEG25 6 coated nanoMOFs; orange: DEX-ALN50-PEG50 7 coated nanoMOFs; gray: DEX-ALN25-PEG75 8 coated nanoMOFs); C-E: TEM images of uncoated nanoMOFs (C), DEX-ALN50-PEG50 7 coated nanoMOFs (D) and DEX-ALN25-PEG75 8 coated nanoMOFs (E); scale bar (200 nm). The mass ratios DEX-ALN-PEG: nanoMOFs were 1:1.

These studies showed that the amount of DEX-ALN-PEG associated to the nanoMOFs was not significantly affected by the ratio of ALN used in the experiments. This suggests that a large number of ALN moieties are not required for an efficient coating of the nanoMOFs, and that DXT-ALN25-PEG75 8 already shows enough ALN appendages (~5) to perform the most efficient coating we could observed.

The MIL-100(Fe) nanoMOFs coated or not with DEX-ALN-PEG were characterized by a set of complementary techniques. First, XRPD studies indicated that the crystalline structure of MIL-100(Fe) nanoMOFs was preserved after surface modification (Fig. 1B) in spite of the high amounts of DEX-ALN-PEG associated to the NPs. This indicates that functionalization of DEX-ALN-PEG polymers did not disturb the crystalline structure of nanoMOFs. Second, TEM experiments showed that the nanoMOFs maintained their facetted morphology, regardless of the type of DEX-ALN-PEG adsorbed (Fig. 1C-E).

The hydrodynamic diameters of MIL-100(Fe) nanoMOFs were determined by dynamic light scattering (DLS) in water before and after surface modification. The mean hydrodynamic diameter of nanoMOFs before coating was 191 ± 23 nm. Whatever the amount and type of DEX-ALN-PEG coating material, there were no significant mean size and polydispersity variations after the coating process. Final mean diameters were in the range of 193 ± 21 nm to 209 ± 31 nm, indicating that the coating thickness was less than 10 nm and that no aggregation occurred.

Uncoated nanoMOFs had a tendency to aggregate upon storage in water (Fig. 2A), in agreement with previous studies (Agostoni et al., 2015). In contrast, nanoMOFs coated with all the DEX-ALN-PEG samples (mass ratio DEX-ALN-PEG:nanoMOFs 1:1) were stable in water up to three weeks storage, showing that their coating efficiently prevented their aggregation. However, the mass ratios DEX-ALN-PEG:nanoMOFs play an important role on the colloid stability of the nano- MOFs. For example, when reducing 4 fold the amount of DEX-ALN50- PEG50 7 at the nanoMOFs surface (mass ratio DEX-ALN-PEG:nanoMOFs 1:4), aggregation was observed during storage in water, as shown by a diameter increase from 193 nm to more than 400 nm in 24 h (Fig. 2A), possibly due to DEX-ALN-PEG at the surface of nanoMOFs inducing a bridging effect. Therefore this sample was excluded in the following experiments. All the nanoMOFs formulations were stable in the biological medium used in this study (DMEM complemented with 10% FBS) (Fig. 2B). No aggregation was found and the mean diameters remained constant over more than 6 h incubation at 37 °C, allowing for further biological investigations of interactions with macrophages.

To prove that the DEX-ALN-PEG copolymer did not penetrate inside the nanostructure, we performed drug encapsulation. Briefly, DOX, an anticancer drug, was used as a guest molecule for drug loading studies. DOX was efficiently loaded in uncoated nanoMOFs by host-guest interactions by adapting a previously reported procedure (Anand et al., 2014). DOX-loaded nanoMOFs were further surface-modified with DEX-ALN-PEG copolymers. It was shown that coating with DEX-ALNPEG copolymers did not induce any DOX release (< 2 ± 0.3%), indicating that DEX-ALN-PEG copolymer did not interfere with the drug molecules located inside the porous cores.

3.2.2. Surface properties of nanoMOFs before and after functionalization

ZP measurements were performed to gain insights on the influence of the coatings on the global charge of the NPs. The ZP of the nanoMOFs, coated or not, was found to be strongly

dependent upon the Fig. 1. Preparation and characterization of nanoMOFs coated or not with DEX-ALN-PEG. A: schematic representation of the «green» preparation of DEX-ALN-PEG coated nanoMOFs in water; For DEX-ALN-PEG, the red balls represent alendronate (ALN) moieties, dextran (DEX) is represented in yellow and poly(ethylene glycol) (PEG) chains are in white. B: XRPD patterns of nanoMOFs coated or not with DEX-ALN-PEG (green: nanoMOFs; purple: DEX-ALN75-PEG25 6 coated nanoMOFs; orange: DEX-ALN50-PEG50 7 coated nanoMOFs; gray: DEX-ALN25-PEG75 8 coated nanoMOFs); C-E: TEM images of uncoated nanoMOFs (C), DEX-ALN50-PEG50 7 coated nanoMOFs (D) and DEX-ALN25-PEG75 8 coated nanoMOFs (E); scale bar (200 nm). The mass ratios DEX-ALN-PEG: nanoMOFs were 1:1.

pH of the suspension medium, in a range of 1 to 10 (Fig. 3A). Typically, the ZP of uncoated nanoMOFs was positive (+23 ± 3 mV) at pH 5, whereas it shifted to negative values (-15 ± 3 mV) at pH 7. This was attributed to the presence at the nanoMOFs external surface of both uncoordinated iron sites and terminal COOH groups from the nanoMOF linker (trimesic acid, pKa's=3.16, 3.98, and 4.85). The ZP values varied after coating with DEX-ALN-PEG copolymers (Fig. 3A). At acidic pH (< 4), the ZP was close to zero (-3 to 3 mV) indicating that the surface groups on the nanoMOFs were shielded by the coating material. At basic pH (> 7) the ZP values of -15 ± 5 mV were similar to those previously reported for DEX coatings (Lemarchand et al., 2005). Of note, there was no significant variation for ZP values obtained with the different DEX-ALN-PEG copolymers, except in the case of the copolymer with the highest PEG content (DEX-ALN25-PEG75 8) whose ZP values were the closest to zero. This is in line with the protective effect of PEG shells on NPs, as previously reported (Rouzes, Gref, Leonard, Delgado, & Dellacherie, 2000). It is well known that surface functionalization strongly influences the biodistribution of the nanocarriers (Gref et al., 1995). Indeed, after intravenous administration of NPs, plasma proteins readily adsorb on the external surface of the NPs, creating the so-called "protein corona", which considerably affects the NPs physicochemical properties and in vivo fate (Gref et al., 2000). To gain further understanding on protein adsorption, the interaction of nanoMOFs, coated or not with DEX-ALNPEG, with HSA, the most abundant protein in human blood plasma, was studied here. Indeed, for many other types of NPs, HSA was used as model protein to investigate the capacity of PEG coatings to reduce protein adsorption (Gref et al., 2000).

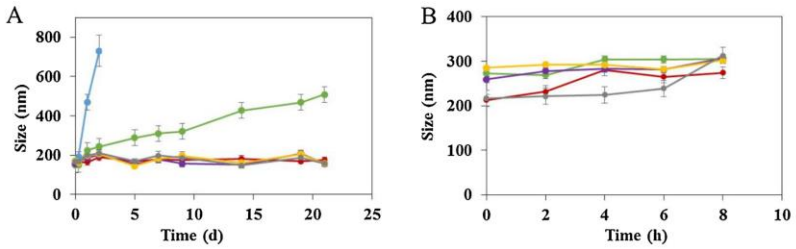


Fig. 2. Stability of nanoMOFs coated or not with DEX-ALN-PEG in water (A) and in DMEM cell culture medium (B). Green: uncoated nanoMOFs; purple: nanoMOFs coated with DEX-ALN_{75}-PEG_{25} **6** (mass ratio DEX-ALN-PEG:nanoMOFs 1:1); orange: nanoMOFs coated with DEX-ALN_{50}-PEG_{50} **7** (mass ratio DEX-ALN-PEG:nanoMOFs 1:1); gray: nanoMOFs coated with DEX-ALN_{25}-PEG_{75} **8** (mass ratio DEX-ALN-PEG:nanoMOFs 1:1); blue: nanoMOFs coated with DEX-ALN_{50}-PEG_{50} **7** (mass ratio DEX-ALN-PEG:nanoMOFs 1:4); red: nanoMOFs coated with DEX-ALN_{50}-PEG_{50} **7** (mass ratio DEX-ALN-PEG: nanoMOFs 1:2).

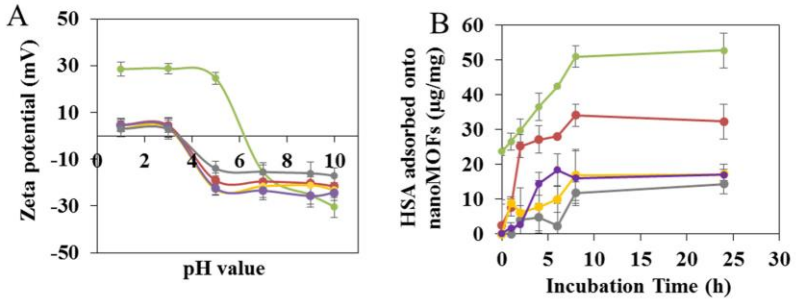
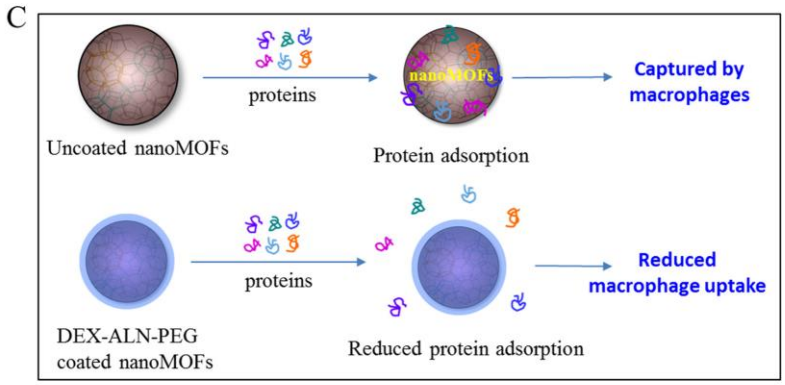


Fig. 3. Effect of surface modification of nanoMOFs by DEX-ALN-PEG copolymers on their ZP (A), amounts of HSA adsorbed (B), and a schema explaining the HSA adsorption (C). Green: uncoated nanoMOFs; purple: nanoMOFs coated with DEX-ALN_{75}-PEG_{25} **6** (mass ratio DEX-ALN-PEG: nanoMOFs 1:1); orange: nanoMOFs coated with DEX-ALN_{50}-PEG_{50} **7** (mass ratio DEX-ALN-PEG: nanoMOFs 1:1); gray: nanoMOFs coated with DEX-ALN_{25}-PEG_{75} **8** (mass ratio DEX-ALN-PEG: nanoMOFs 1:1); red: nanoMOFs coated with DEX-ALN_{50}-PEG_{50} **7** (mass ratio DEX-ALN-PEG: nanoMOFs 1:2).



NanoMOFs coated or not with DEX-ALN-PEG copolymers were incubated with HSA aqueous solutions and the adsorbed HSA amounts, expressed as µg/mg of nanoMOFs, were determined (Fig. 3B). The experiments were carried out with fixed concentrations of nanoMOFs (300 µg/mL) and HSA (100 µg/mL) aqueous solutions. Non-adsorbed HSA was recovered in the supernatant after centrifugation, followed by quantification using a BCA assay. In the case of uncoated nanoMOFs, the amount of adsorbed HSA reached a plateau within 6 h, with around 50 µg HSA/mg nanoMOFs (Fig. 3B). Fig. 2. Stability of nanoMOFs coated or not with DEX-ALN-PEG in water (A) and in DMEM cell culture medium (B). Green: uncoated nanoMOFs; purple: nanoMOFs coated with DEX-ALN75-PEG25 6 (mass ratio DEX-ALNPEG: nanoMOFs 1:1); orange: nanoMOFs coated with DEX-ALN50-PEG50 7 (mass ratio DEX-ALN-PEG:nanoMOFs 1:1); gray: nanoMOFs coated with DEX-ALN25-PEG75 8 (mass ratio DEX-ALN-PEG:nanoMOFs 1:1); blue: nanoMOFs coated with DEX-ALN50- PEG50 7 (mass ratio DEX-ALN-PEG:nanoMOFs 1:4); red: nanoMOFs coated with

DEX-ALN50- PEG50 7 (mass ratio DEX-ALN-PEG: nanoMOFs 1:2). Fig. 3. Effect of surface modification of nanoMOFs by DEX-ALN-PEG copolymers on their ZP (A), amounts of HSA adsorbed (B), and a schema explaining the HSA adsorption (C). Green: uncoated nanoMOFs; purple: nanoMOFs coated with DEX-ALN75-PEG25 6 (mass ratio DEX-ALN-PEG: nanoMOFs 1:1); orange: nanoMOFs coated with DEX-ALN50- PEG50 7 (mass ratio DEX-ALN-PEG: nanoMOFs 1:1); gray: nanoMOFs coated with DEX-ALN25- PEG75 8 (mass ratio DEX-ALN-PEG: nanoMOFs 1:1); red: nanoMOFs coated with DEX-ALN50-PEG50 7 (mass ratio DEX-ALN-PEG: nanoMOFs 1:2). G. Cutrone, et al. *Carbohydrate Polymers 223 (2019) 115085* 9 Surface modification with DEX-ALN-PEG significantly reduced HSA adsorption, with ∼35 μg HSA/mg nanoMOFs for the case of DEXALN50-PEG50 7 (mass ratio DEX-ALN-PEG:nanoMOFs 1:2) coatings. This amount was further reduced to less than 20 μg HSA/mg nanoMOFs for the coatings with DEX-ALN75-PEG25 6, DEX-ALN50-PEG50 7, and DEX-ALN25-PEG75 8 (mass ratio DEX-ALN-PEG:nanoMOFs 1:1). There results clearly show that the DEX-ALN-PEG coatings are able to reduce the adsorption of the model protein HSA. This indicates that the surface modification with DEX-ALN-PEG copolymers potentially reduce the protein adsorption (e.g the opsonisation), which plays an important role on macrophage uptake (Fig. 3C).

3.2.3. Macrophage uptake of DEX-ALN-PEG surface modified nanoMOFs

The capacity of DEX-ALN-PEG coated nanoMOFs to escape macrophage uptake was evaluated on the murine macrophage J774A.1 cell line. NanoMOFs were colored using an iron staining procedure (see material and methods), allowing their identification inside cells by optical microscopy. To complete these qualitative studies, quantitative data on the amounts of nanoMOFs internalized in cells were obtained by ICP-MS, after extensive washing to remove the non-associated particles.

According to a lactic acid dehydrogenase (LDH) test previously performed to study nanoMOFs toxicity (Li et al., 2019), the particles used here coated or not with DEX-ALN-PEG shells were nontoxic for the J774A.1 cells up to 100 μg/mL, with more than 80% cell viability. This is in agreement with previously reported data showing the lack of toxicity of MIL-100(Fe) nanoMOFs (Baati et al., 2013; Bellido et al., 2015; Giménez-Marqués et al., 2018; Horcajada et al., 2010; Li et al., 2019). Internalization kinetics of nanoMOFs in J774A.1 macrophages were studied and a typical example is presented in Figure S14 (supplementary material). The amount of internalized uncoated nanoMOFs was quantified by

ICP-MS, showing that after 2 h incubation ~14 µg of uncoated nanoMOFs were taken up in 3×105 J774A.1 macrophages, corresponding to around 1×107 uncoated nanoMOFs/cell and to 47% of the initial uncoated nanoMOFs (Figure S14). Moreover, this amount almost doubled after 4 h incubation, reaching 23 µg uncoated nano- MOFs/3×105 cells (77% of the nanoMOFs), thus demonstrating that macrophages avidly take up uncoated nanoMOFs. Remarkably, the presence of the DEX-ALN-PEG coating significantly reduced the nano-MOFs internalization, whatever the incubation time. For example, there was only less than 3 µg of coated nanoMOFs in 3×105 J774A.1 macrophages (corresponding to 10% of the initial coated nanoMOFs) after 2 h incubation. Even after 4 h incubation, the internalized amount of coated nanoMOFs was still less than 25%.

These direct quantification data obtained by ICP MS were supported by optical investigations of the cells after incubation with the nanoMOFs (Fig. 4). Before contact with nanoMOFs, J774A.1 cells presented a homogeneous morphology with round shapes (Fig. 4A). A typical image showing the massive uptake of uncoated nanoMOFs is presented in Fig. 4B. After 2 h incubation, the nanoMOFs appeared clustered inside the macrophages, mostly at their periphery. In contrast, after the same incubation time, the uptake of DEX-ALN75-PEG25 6 coated nanoMOFs was dramatically reduced (Fig. 4C).

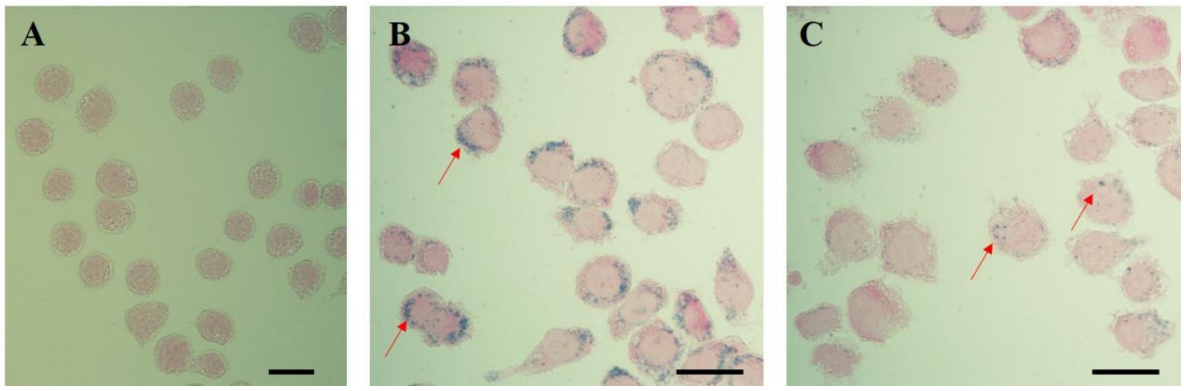


Fig. 4. Optical microscopy images showing the effect of DEX-ALN-PEG coatings on J774 macrophage uptake. **A**: Control J774 macrophages with no treatment; **B**: J774 macrophages after 2 h incubation with 50 µg/mL uncoated nanoMOFs; **C**: J774 macrophages after 2 h incubation with 50 µg/mL DEX-ALN_{75}-PEG_{25} **6** coated nanoMOFs. Red arrows point out nanoMOFs stained using Prussian blue. Scale bar represents 20 □m.

The higher uptake of DEX-ALN75-PEG25 6 coated nanoMOFs after 4 h as compared to 2 h (Figure. S14) could be possibly due to a progressive saturation of the cells and/or a detachment of the coating in the complex biological media containing proteins or by contact

with cell membranes. To further compare the different DEX-ALN-PEG coatings, an incubation time of 4 h was chosen as it corresponds to the blood circulation time of PEG-coated NPs (Gref et al., 1994). Fig. 5 shows the effect of the DEX-ALN-PEG coatings upon macrophage uptake. The nanoMOFs amounts associated to the cells were 39, 32 and 24% for DEX-ALN75-PEG25 6, DEX-ALN50-PEG50 7, and DEX-ALN25-PEG75 8, respectively. This shows that the higher the PEG contents in the coating material, the lower the nanoMOFs uptake. To the best of our knowledge, these are the first quantitative data on PEG-coated nanoMOFs uptake by macrophages based on a direct quantification and visualization of the Fe content in the cells. In comparison, another recent study dealt with nanoMOFs interaction with Raw 246.7 macrophages (Giménez-Marqués et al., 2018). In that case, the MIL-100(Fe) nanoMOFs were coated with PEG by GraftFast, whereas a radiolabeled drug, tritiated gemcitabine monophosphate, was incorporated into the particles. In the presence of coated particles, the detected amount of drug in the cells was reduced, as opposed to uncoated ones. However, this study did not take into account drug release during incubation with the cells, which may have influenced the quantity of drug detected as permeated into the cells (Rodriguez-Ruiz et al., 2015).

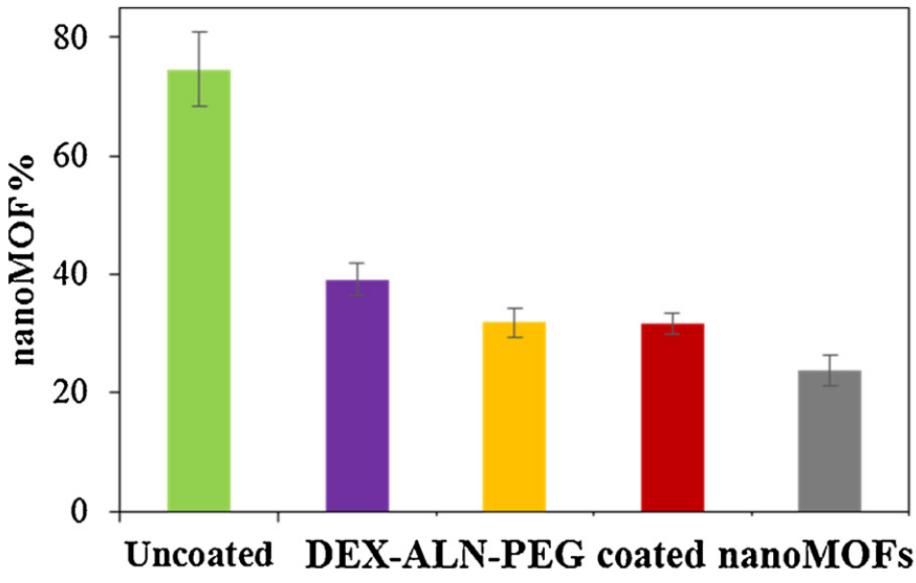


Fig. 5. In vitro interaction of nanoMOFs, coated or not with with a J774A.1 macrophage cell line. Purple: nanoMOFs coated with DEX-ALN75-PEG25 6 (mass ratio DEX-ALN-PEG:nanoMOFs 1:1); Orange: nanoMOFs coated with DEXALN50- PEG50 7 (mass ratio DEX-ALN-PEG:nanoMOFs 1:1); red: nanoMOFs coated with DEX-ALN50-PEG50 7 (mass

ratio DEX-ALN-PEG:nanoMOFs 1:2); gray: nanoMOFs coated with DEX-ALN25-PEG75 8 (mass ratio DEX-ALNPEG: nanoMOFs 1:1). 50 μg/mL nanoMOFs were incubated with 3×105 J774A.1 cells for 4 h, then washed to remove the loosely adhering particles. After cell lysis, the amount of internalized nanoMOFs was determined by ICPMS and was expressed as a % of the initial amount put in contact with the cells.

4. Conclusions

DEX-ALN-PEG copolymers were successfully synthesized, controlling both the PEG and ALN grafting densities ranging from 75:25 to 25:75 ratios. They spontaneously adhered onto the external surface of MIL-100(Fe) nanoMOFs in aqueous media, forming a stable coating. In turn, the coating ensured the stability of the nanoMOFs upon storage and enabled to reduce by a 3 fold the in vitro uptake by macrophages. Further studies will deal with the effect on the drug release, further engineering of the coating by grafting specific ligands and/or fluorescent molecules, and coating on other metal-based MOFs (such as rare earth MOFs that can be used in biomedical applications). The in vivo fate of DEX-ALN-PEG functionalized nanoMOFs will be investigated.

Author contributions

The authors have made the following declarations about their contributions: Conceived and designed the experiments: RG, AVB, DD Performed the experiments: GC, JQ, AA, XL, MMM, DF, JMCS, BMA, JRE Contributed reagents/materials/analysis tools: GC, AA, CL, XL, JQ, MMM, JMCS, DD, RG, AVB Performed data analysis: GC, RG, AVB, DD, CL, XL, MMM, JMCS Wrote the paper: RG, AVB, XL, GC G. Cutrone and J. Qiu equally contributed to this work.

Declaration of Competing Interest

The authors declare no conflict of interest.

Acknowledgments

Financial support for this work was provided by the European Union through FP7-PEOPLE-2013-ITN (http://itn-cyclonhit.eu) project (Grant Agreement no. 608407), the French National Research Agency (ANR- 14-CE08-0017 and ANR-16-CE18-0018) and the Spanish Ministry of Economy and Competitiveness (Grants CTQ2017-90050-R and CTQ2016-79412-P). This work was also supported by a public grant overseen by the French National Research Agency

as part of the “Investissements d’Avenir” program (Labex NanoSaclay, ANR-10-LABX-0035). We acknowledge Dr. Doru Constantin for help with XRPD experiments. We are grateful to Ludivine Houel Renault for help with the cell culture facility in Centre Laser de l'Université Paris-Sud (CLUPS). This work has benefited from the facilities and expertise of the Liquid Chromatography Platform (Institut de Chimie de Lyon) for the characterization of polymers.

Appendix A. Supplementary data

Supplementary material related to this article can be found, in the online version, at doi:https://doi.org/10.1016/j.carbpol.2019.115085.

References

Abdelhameed, R. M., Rehan, M., & Emam, H. E. (2018). Figuration of Zr-based MOF@ cotton fabric composite for potential kidney application. Carbohydrate Polymers, 195, 460–467.

Agostoni, V., Anand, R., Monti, S., Hall, S., Maurin, G., Horcajada, P., et al. (2013). Impact of phosphorylation on the encapsulation of nucleoside analogues withinporous iron(III) metal–organic framework MIL-100(Fe) nanoparticles. Journal ofMaterials Chemistry B, 1, 4231–4242.

Agostoni, V., Chalati, T., Horcajada, P., Willaime, H., Anand, R., Semiramoth, N., et al. (2013). An improved anti-HIV activity of NRTI via metal-organic frameworks nanoparticles. Advanced Healthcare Materials, 2, 1630–1637.

Agostoni, V., Horcajada, P., Noiray, M., Malanga, M., Aykaç, A., Jicsinszky, L., et al. (2015). A “green” strategy to construct non-covalent, stable and bioactive coatings on porous MOF nanoparticles. Scientific Reports, 5, 7925.

Alemán, E. A., Pedini, H. S., & Rueda, D. (2009). Covalent bond-based immobilization approaches for single-molecule fluorescence. ChemBiochem, 10, 2862–2866.

Anand, R., Borghi, F., Manoli, F., Manet, I., Agostoni, V., Reschiglian, P., et al. (2014). Host-guest interactions in Fe(III)-trimesate MOF nanoparticles loaded with doxorubicin. The Journal of Physical Chemistry B, 118, 8532–8539.

Aykaç, A., Noiray, M., Malanga, M., Agostoni, V., Casas-Solvas, J. M., Fenyvesi, É., et al. (2017). A non-covalent “click chemistry” strategy to efficiently coat highly porousMOF nanoparticles with a stable polymeric shell. Biochimica et Biophysica Acta -General Subjects, 1861, 1606–1616.

Baati, T., Njim, L., Neffati, F., Kerkeni, A., Bouttemi, M., Gref, R., et al. (2013). In depth analysis of the in vivo toxicity of nanoparticles of porous iron(III) metal-organic frameworks. Chemical Science, 4, 1597–1607.

Barceloux, D. G. (1999). Copper. Clinical Toxicology, 37, 217–230. Barenholz, Y. (2012). Doxil® - the first FDA-approved nano-drug: Lessons learned. Journal of Controlled Release, 160, 117–134.

Bellido, E., Hidalgo, T., Lozano, M. V., Guillevic, M., Simón-Vázquez, R., Santander-Ortega, M. J., et al. (2015). Heparin-engineered mesoporous iron metal-organic framework nanoparticles: Toward stealth drug nanocarriers. Advanced Healthcare Materials, 4, 1246–1257.

Biaglow, J. E., Manevich, Y., Uckun, F., & Held, K. D. (1997). Quantitation of hydroxyl radicals produced by radiation and copper-linked oxidation of ascorbate by 2-deoxy-D-ribose method. Free Radical Biology & Medicine, 22, 1129–1138.

Chen, D., Yang, D., Dougherty, C. A., Lu, W., Wu, H., He, X., et al. (2017). In vivo targeting and positron emission tomography imaging of tumor with intrinsically radioactive metal-organic frameworks nanomaterials. ACS Nano, 11, 4315–4327.

Di Nunzio, M. R., Agostoni, V., Cohen, B., Gref, R., & Douhal, A. (2014). A "ship in a bottle" strategy to load a hydrophilic anticancer drug in porous metal organic framework nanoparticles: Efficient encapsulation, matrix stabilization, and photodelivery. Journal of Medicinal Chemistry, 57, 411–420.

Giménez-Marqués, M., Bellido, E., Berthelot, T., Simón-Yarza, T., Hidalgo, T., Simón-Vázquez, R., et al. (2018). GraftFast surface engineering to improve MOF nanoparticles furtiveness. Small, 14, 1801900.

Grandjean, C., Boutonnier, A., Guerreiro, C., Fournier, J. M., & Mulard, L. A. (2005). On the preparation of carbohydrate-protein conjugates using the traceless Staudinger ligation. The Journal of Organic Chemistry, 70, 7123–7132.

Gref, R., Domb, A., Quellec, P., Blunk, T., Müller, R. H., Verbavatz, J. M., et al. (1995). The controlled intravenous delivery of drugs using PEG-coated sterically stabilized nanospheres. Advanced Drug Delivery Reviews, 16, 215–233.

Gref, R., Lück, M., Quellec, P., Marchand, M., Dellacherie, E., Harnisch, S., et al. (2000). "Stealth" corona-core nanoparticles surface modified by polyethylene glycol (PEG): Influences of the corona (PEG chain length and surface density) and of the core composition on phagocytic uptake and plasma protein adsorption. Colloids and Surfaces B, Biointerfaces, 18, 301–313.

Gref, R., Minamitake, Y., Peracchia, M. T., Trubetskoy, V., Torchilin, V., & Langer, R. (1994). Biodegradable long-circulating polymeric nanospheres. Science, 263, 1600–1603.

Horcajada, P., Chalati, T., Serre, C., Gillet, B., Sebrie, C., Baati, T., et al. (2010). Porous metal–organic-framework nanoscale carriers as a potential platform for drug delivery and imaging. Nature Materials, 9, 172–178.

Horcajada, P., Gref, R., Baati, T., Allan, P. K., Maurin, G., Couvreur, P., et al. (2012). Metal-organic frameworks in biomedicine. Chemical Reviews, 112, 1232–1268.

Hoskins, B. F., & Robson, R. (1989). Infinite polymeric frameworks consisting of three dimensionally linked rod-like segments. Journal of the American Chemical Society, 111, 5962–5964.

Ke, J., Dou, H., Zhang, X., Uhagaze, D. S., Ding, X., & Dong, Y. (2016). Determination of pKa values of alendronate sodium in aqueous solution by piecewise linear regression based on acid-base potentiometric titration. Journal of Pharmaceutical Analysis, 6, 404–409.

Kuil, J., Branderhorst, H. M., Pieters, R. J., De Mol, N. J., & Liskamp, R. M. J. (2009). ITAM-derived phosphopeptide-containing dendrimers as multivalent ligands for Syk tandem SH2 domain. Organic & Biomolecular Chemistry, 7, 4088–4094.

Lemarchand, C., Gref, R., Lesieur, S., Hommel, H., Vacher, B., Besheer, A., et al. (2005). Physico-chemical characterization of polysaccharide-coated nanoparticles. Journal of Controlled Release, 108, 97–111.

Li, X., Semiramoth, N., Hall, S., Tafani, V., Josse, J., Laurent, F., et al. (2019). Compartmentalized encapsulation of two antibiotics in porous nanoparticles: An efficient strategy to treat intracellular infections. Particle & Particle Systems Characterization, 36, 1800360.

Liu, G., Li, L., Xu, D., Huang, X., Xu, X., Zheng, S., et al. (2017). Metal-organic framework preparation using magnetic graphene oxide-β-cyclodextrin for neonicotinoid pesticide adsorption and removal. Carbohydrate Polymers, 175, 584–591.

Notni, J., & Wester, H. J. (2016). A practical guide on the synthesis of metal chelates for molecular imaging and therapy by means of click chemistry. Chemistry - A European Journal, 22, 11500–11508.

Oms, O., Yang, S., Salomon, W., Marrot, J., Dolbecq, A., Rivière, E., et al. (2016). Heteroanionic materials based on copper clusters, bisphosphonates, and polyoxometalates: Magnetic properties and comparative electrocatalytic NOx reduction studies. Inorganic Chemistry, 55, 1551–1561.

Ostović, D., Stelmach, C., & Hulshizer, B. (1993). Formation of a chromophoric complex between alendronate and copper (II) ions. Pharmaceutical Research, 10, 470–472.

Perrin, D. D., & Armarego, W. F. L. (1989). Purification of laboratory chemicals (3rd ed.). Oxford: Pergamon.

Rodriguez-Ruiz, V., Maksimenko, A., Anand, R., Monti, S., Agostoni, V., Couvreur, P., et al. (2015). Efficient “green” encapsulation of a highly hydrophilic anticancer drug in metal-organic framework nanoparticles. Journal of Drug Targeting, 23, 759–767.

Rouzes, C., Gref, R., Leonard, M., De Sousa Delgado, A., & Dellacherie, E. (2000). Surface modification of poly(lactic acid) nanospheres using hydrophobically modified dextrans as stabilizers in an o/w emulsion/evaporation technique. Journal of Biomedical Materials Research, 50, 557–565.

Semple, J. E., Sullivan, B., Vojkovsky, T., & Sill, K. N. (2016). Synthesis and facile endgroup quantification of functionalized PEG azides. Journal of Polymer Science Part A: 11 Polymer Chemistry, 54, 2888–2895.

Simon-Yarza, M. T., Baati, T., Paci, A., Lesueur, L. L., Seck, A., Chiper, M., et al. (2016). Antineoplastic Busulfan encapsulated in metal organic framework nanocarrier: First in vivo results. Journal of Materials Chemistry B, 4, 585–588.

Simon-Yarza, T., Baati, T., Neffati, F., Njim, L., Couvreur, P., Serre, C., et al. (2016). In vivo behavior of MIL-100 nanoparticles at early times after intravenous administration. International Journal of Pharmaceutics, 511, 1042–1047.

Simon-Yarza, T., Giménez-Marqués, M., Mrimi, R., Mielcarek, A., Gref, R., Horcajada, P., et al. (2017). A smart metal-organic framework nanomaterial for lung targeting. Angewandte Chemie International Edition, 56, 15565–15569.

Su, Y., Li, L., Wang, H., Wang, X., & Zhang, Z. (2016). All-in-One azides: Empowered click reaction for in vivo labeling and imaging of biomolecules. Chemical Communication, 52, 2185–2188.

Sun, G., Lin, X., Wang, Z., Feng, Y., Xu, D., & Shen, L. (2011). PEGylated inulin as longcirculating pharmaceutical carrier. Journal of Biomaterials Science Polymer Edition, 22,

429–441.

Yuan, S., Feng, L., Wang, K., Pang, J., Bosch, M., Lollar, C., et al. (2018). Stable metalorganic frameworks: Design, synthesis, and applications. Advanced Materials, 30, 1–35.

Zhang, H. H., Hu, H., Zhang, H. H., Dai, W., Wang, X., Wang, X., et al. (2015). Effects of PEGylated paclitaxel nanocrystals on breast cancer and its lung metastasis. Nanoscale, 7, 10790–10800.

Zimpel, A., Preiß, T., Röder, R., Engelke, H., Ingrisch, M., Peller, M., et al. (2016). Imparting functionality to MOF nanoparticles by external surface selective covalent attachment of polymers. Chemistry of Materials, 28, 3318–3326.

Zhu, X., Gu, J., Wang, Y., Li, B., Li, Y., Zhao, W., et al. (2014). Inherent anchorages in UiO-66 nanoparticles for efficient capture of alendronate and its mediated release. Chemical Communication, 50, 8779–8782.